Detection of Electronic and Vibrational Coherence Effects in Electron-Transfer Systems by Femtosecond Time-Resolved Fluorescence Spectroscopy: Theoretical Aspects

A. V. Pisliakov,*,† M. F. Gelin,‡ and W. Domcke†

Institute of Physical and Theoretical Chemistry, Technical University of Munich, Lichtenbergstrasse 4, 85747 Garching, Germany, and Institute of Molecular and Atomic Physics, National Academy of Sciences of Belarus, Skaryna Avenue 70, Minsk 220072, Belarus

Received: November 19, 2002; In Final Form: February 13, 2003

Time- and frequency-gated spontaneous emission signals are calculated for electron-transfer systems. The electron-transfer dynamics is modeled in terms of two diabatic excited electronic states which are electronically coupled as well as strongly coupled to a reaction mode, which in turn is weakly coupled to a dissipative environment. The bath degrees of freedom are integrated out in the framework of Redfield theory. The reduced density matrix is obtained by the numerical solution of the Redfield equations of motion. For suitably chosen parameters, the model describes interesting features of ultrafast electron-transfer dynamics such as electronic beatings (due to the electronic coherence) and steplike electronic population decay (due to vibrational coherence). The relationship between the intrinsic system dynamics and the time-resolved fluorescence (from the electronically coupled excited states to the ground state) is investigated. The time- and frequency-gated fluorescence spectra are obtained for various durations of the pump and gate pulses. For suitably chosen parameters of the pump and gate pulses, the signal maps the vibrational wave packet dynamics of the electron-transfer system. The frequency-integrated time-resolved fluorescence, on the other hand, reflects directly the population dynamics of the diabatic electronic states. It is shown that the step structures in the electronic population probability due to vibrationally coherent electron transfer or the oscillatory structures due to electronic coherence can be experimentally detected, provided the duration of the pump and gate pulses is of the order of a vibrational period or electronic beating period, or shorter. When the duration of the pulses significantly exceeds the vibrational or electronic beating periods, the system-specific features are averaged out, resulting in exponential electronic population decay corresponding to the electron-transfer rate.

1. Introduction

With the availability of femtosecond pulses,[1,2] various time-resolved spectroscopic techniques enable one to observe the evolution of spectra in "real time", and thus to monitor microscopic nuclear motion and the most elementary processes of chemical dynamics which take place on ultrafast time scales.[3−7] Among these techniques, the time- and frequency-gated (TFG) spontaneous emission (SE) spectroscopy has an important advantage over, e.g., diverse pump−probe techniques. Indeed, if the excitation and gate pulses do not overlap, the SE consists solely of the fluorescence component, which directly monitors the ultrafast excited-state dynamics. The technical realization of TFG SE spectroscopy is the fluorescence up-conversion technique,[8−12] in which the SE and a short up-conversion (or time gate) pulse are mixed in a nonlinear crystal, and the integrated intensity of the sum frequency is monitored. The time resolution is achieved because the gate pulse creates a "time window" for SE, and the frequency resolution is achieved by dispersing the up-converted signal in a monochromator or "frequency filter". The TFG SE (which is also often called "time-resolved fluorescence spectroscopy") has become an effective tool for the monitoring of the excited-state dynamics of various systems ranging from isolated diatomic molecules to rather complex systems (carotenoids, chromophore-solvent systems, or porphyrins).[4,13−18]

When ultrafast TFG SE experiments are interpreted, a fundamental question arises: how can one extract quantitative information on the system dynamics from the measured signals? There is a certain gap between theoretical and experimental results. Theorists prefer to calculate quantities such as the time-dependent electronic population probability or various correlation functions, while experimentalists measure certain time-dependent transients. Indeed, it is generally assumed that the measured TFG SE signal maps the excited-state population dynamics. But the question is, which population (diabatic or adiabatic) and to which extent? Clearly, the experimental transients are indirectly connected with the electronic population dynamics and are strongly influenced by the detection process. Thus, for systems with complicated and ultrafast dynamics, it is necessary to introduce explicitly the description of the TFG procedure into the theory and to establish rigorously the connection of the experimentally measured signals with the underlying microscopic dynamics. In the present article, we study this issue for the case of ultrafast electron-transfer (ET) systems which, due to a strong nonadiabatic coupling, exhibit ultrafast decay dynamics.[19]

One of the most fundamental questions, which is addressed when discussing ultrafast ET reactions, is the manifestation of various coherences in the population dynamics and measured responses. It has been shown theoretically that coherent effects

* Corresponding author. E-mail: pisliakov@ch.tum.de.
† Technical University of Munich.
‡ National Academy of Sciences of Belarus.

10.1021/jp027491p CCC: $25.00
Published on Web 03/26/2003

in ultrafast ET can be either of vibrational or of electronic nature.[20−30] Therefore, it is necessary to distinguish between these two types of coherences when interpreting particular experiments. Excitation of vibrational modes by a short pump pulse with a broad bandwidth results in a coherent superposition of vibrational levels, i.e., in the creation of a vibrational wave packet (WP) in the excited electronic state. Vibrational coherence (VC) effects in ultrafast ET have been studied theoretically with time-dependent wave packet and reduced density matrix (RDM) techniques (see, e.g., refs 20−26). These calculations have shown that the WP motion in the excited state manifests itself in the time-dependent population dynamics through characteristic steplike structures. Another conclusion of the theoretical analysis[26−30] is that, under certain circumstances, another type of coherence, i.e., electronic coherence (EC), also plays an important role in ultrafast ET. Sufficiently large values of the electronic coupling may result in a coherent electronic motion ("coherent ET" or "back-ET") between donor and acceptor states. The effect of EC, if it is present in the system, can be observed as large-amplitude quantum beatings in the population dynamics,[26−30] which are analogous to the well-known Rabi oscillations in optical physics.[31] Naturally, both EC and VC contribute to the population evolution in the excited state for systems with sufficiently strong electronic coupling and nonstationary preparation. This leads to a complex dynamics with peculiar features, ranging from steplike structures (due to VC) to electronic quantum beats (due to EC). Recent ultrafast spectroscopic measurements have confirmed the persistence of pronounced coherent effects on a picosecond time scale in the ultrafast ET dynamics for various molecular systems, from diatomics to proteins.[3−5,32−35] However, when trying to interpret particular experiments, it is not entirely clear if the measured oscillatory patterns are to be attributed to vibrational or electronic coherences. So, it is of considerable importance to clarify (i) which types of coherences are responsible for the excited-state dynamics and can, therefore, be observed through TFG SE responses for real systems and (ii) how to separate the two types of coherences.

A number of papers has appeared in recent years, in which the problem of ultrafast ET has been treated at different levels of sophistication. Of particular relevance to the present consideration are the contributions presented in refs 24, 25, and 36−44. The present work is a generalization of an earlier paper by Jean,[36] extending the theory beyond bare time- and frequency-resolved spectra. It shares the general methodology with recent papers by Matro and Cina[38] and Mukamel and collaborators[43,44] (preparation by a pump pulse of finite duration, explicit consideration of the TFG procedure, reduced density-matrix description of the nonadiabatic excited-state dynamics within the Redfield theory, the doorway−window formalism). A novel feature of the present work is the consideration of several carefully selected ET model systems exhibiting EC and/or VC and the systematic exploration of the effects of the preparation and SE detection by pulses of finite duration. In particular, we want to answer the following fundamental questions: (i) To which extent is the intrinsic system dynamics reflected by TFG SE spectra? (ii) What are the requirements on the system preparation and detection procedure in order to observe electronic, vibrational, or combined coherences in TFG SE experiments?

The paper is organized as follows. A brief summary of TFG SE theory and explicit expressions for the signals are presented in section 2. The ET model is introduced in section 3. In that section we also give the equations (Redfield theory) used for the calculation of the system dynamics. Section 4 contains the results of calculations of TFG spectra for this ET model. The effects of temporal resolution and pump-pulse duration are studied. The manifestation of various coherences in the signal is also discussed. Concluding remarks are contained in section 5.

For notational convenience, we use units in which $\hbar = 1$.

2. TFG SE Spectra

The total intensity of the temporally gated and spectrally filtered field at the position $\vec{r}$ in the far-field region is given by the general expression[47−49]

$$S_{st}(t_0,\omega_0) \sim \int_{-\infty}^{\infty} dt \int_{-\infty}^{\infty} dt' \int_{-\infty}^{\infty} dt'' \, E_t(t';t_0)\, E_t^*(t'';t_0) \times F_s(t-t',\omega_0)\, F_s^*(t-t'',\omega_0)\, \langle E(\vec{r},t')\, E(\vec{r},t'')^* \rangle \quad (1)$$

Here $E_t(t;t_0)$ is the time-gate function which is strongly peaked near the gating time $t \sim t_0$, the function $F(t-t',\omega_0)$ is responsible for the spectral filtering near the central frequency ω_0, and $\langle E(\vec{r},t')\, E(\vec{r},t'')^* \rangle$ is the correlation function of the emitted field.

For performing explicit calculations, we shall further use the standard approximations[47−50]

$$E_t(t;t_0) = \Gamma^{1/2} \exp(-\Gamma|t - t_0|) \quad (2)$$

for the time gate and

$$F_s(t,\omega_0) = \vartheta(t)\, \frac{\gamma}{2} \exp\{-(\gamma + i\omega_0)t\} \quad (3)$$

for the frequency filter (which is a good approximation for the Fabry−Perot filter[47]). The constants Γ and γ determine the widths of the corresponding filters ($\Gamma = \infty$ and $\gamma = 0$ correspond to an ideal time and frequency resolution, respectively). $\vartheta(t)$ is the Heaviside step function which ensures causality.

For our purposes it is sufficient to consider a system with a single optical transition between the ground (g) and excited (e) electronic states. We write the total Hamiltonian as

$$H = \begin{pmatrix} H_g & 0 \\ 0 & H_e \end{pmatrix} \quad (4)$$

where H_g is the vibrational Hamiltonian of the electronic ground state and H_e describes the excited-state dynamics (e.g., the dynamics of two coupled electronic states).

The standard and universal description of various nonlinear spectroscopic techniques is formulated in terms of the optical response functions.[45] For multidimensional and/or nonadiabatic systems, a straightforward computation of these functions is not feasible. For this reason, it is conventional practice to adopt a system-bath approach, in which a few optically active vibrational modes, which are directly coupled to the electronic transition, constitute the relevant system, while the rest of the inter- and intramolecular modes is treated as a heat bath. Thus, the total Hamiltonian is expressed as a sum of system (S), bath (B), and a system−bath interaction (SB) contributions

$$H_g = H_g^S + H_g^B + H_g^{SB}$$
$$H_e = H_e^S + H_e^B + H_e^{SB} \quad (5)$$

By integrating out the bath degrees of freedom (see section 3), one arrives at the dissipative kinetic equation for the RDM in the excited electronic state

$$\frac{\partial\sigma(t)}{\partial t} = -iL\sigma(t) \tag{6}$$

where, in a general form, L is the Liouvillian. In principle, eq 6 describes the dynamics of the total system (ground + excited electronic states). For our purposes it is sufficient, however, to consider only the excited-state density matrix $\sigma(t)$, because other terms (ground-state electronic population and optical coherences) do not contribute to the fluorescence signal. The RDM $\sigma(t)$ of the excited electronic state is the primary quantity describing the ET dynamics and the fluorescence signal.

If the pump and gate pulses do not overlap, the calculations simplify considerably, because we can employ a convenient doorway−window representation of TFG SE spectrum:[45,49]

$$S_{st}(t_0,\omega_0) \sim Tr[W(\omega_0)\, e^{-iLt_0}\, D(\omega_L)] \tag{7}$$

Here

$$D(\omega_L) = \int_{-\infty}^{\infty} dt' \int_0^{\infty} dt_1\, E_L(t')\, E_L(t'-t_1) \times e^{i\omega_L t_1}\, e^{iH_e^S t}\, e^{-iH_e^S t_1}\, V_{eg}\rho_g\, e^{iH_g^S t_1}\, V_{ge}\, e^{-iH_e^S t'} + HC \tag{8}$$

is the doorway (D) operator and

$$W(\omega_0) = \int_{-\infty}^{\infty} dt \int_0^{\infty} dt_3\, E_t(t+t_3) \times E_t(t)\, e^{(i\omega_0-\gamma)t_3}\, e^{iH_e^S t}\, V_{eg}\, e^{iH_g^S t_3}\, V_{ge}\, e^{-iH_e^S t_3}\, e^{-iH_e^S t} + HC \tag{9}$$

is the window (W) operator, V_{eg} and V_{ge} are the transition dipole operators (system-field interaction is given by $H_{SF}(t) = \vec{\epsilon}\cdot\vec{\mu}\, E(t)\, V(t)$),

$$E_L(t) = \Gamma_L^{1/2}\, e^{-\Gamma_L|t|} \tag{10}$$

is the envelope of the excitation pulse with carrier frequency ω_L,

$$\rho_i \equiv Z_i^{-1}\, e^{-H_i/kT} \tag{11}$$

are the equilibrium vibrational distributions in the ground (i = g) and excited (i = e) states, and Z_i are the corresponding partition functions. In the derivation of eqs 8 and 9, we have made the standard assumption that the excitation and gate pulses are short on the time scale of the system-bath relaxation.[45,46] In this case, no bath-induced excited-state population relaxation occurs during the pump and probe processes, and one can substitute the corresponding total Hamiltonians by their system parts in the D and W operators.

The DW representation is seen to provide a very simple and intuitive picture of the TFG SE measurement. We can think of the fluorescence emission as a stepwise process, which proceeds via optical creation of population in the excited state by the pump pulse (which is defined by the D operator), its subsequent evolution (which is described by the excited-state propagator e^{-iLt_0}), and fluorescence emission (the W operator describes the TFG detection).

To evaluate the D and W functions (8, 9), we introduce the system eigenstates

$$H_g^S|n\rangle = E_n|n\rangle \qquad H_e^S|\alpha\rangle = E_\alpha|\alpha\rangle \tag{12}$$

(hereafter, the eigenvalues and eigenfunctions of H_g^S and H_e^S are denoted by Latin and Greek letters, respectively). The corresponding frequencies read

$$\omega_{\alpha n} = E_\alpha - E_n \qquad \omega_{\alpha\beta} = E_\alpha - E_\beta \tag{13}$$

If we additionally assume that the time-gate function and the pump pulse are of exponential form and described by equations such as (2) and (10), all the time integrations in (8) and (9) can be performed analytically

$$S_{st}(t_0,\omega_0) \sim \sum_{\alpha,\beta,\alpha_1,\beta_1} W_{\alpha\beta}(\omega_0)\, \{e^{-iLt_0}\}_{\alpha_1\beta_1}^{\alpha\beta} D_{\alpha_1\beta_1}(\omega_L) \tag{14}$$

where

$$D_{\alpha\beta}(\omega_L) = \sum_n V_{\alpha n}V_{n\beta}\rho_g(n)\left\{\frac{1}{\Gamma_L - i(\omega_L-\omega_{\alpha n})}\frac{1}{\Gamma_L - i(\omega_L-\omega_{\beta n})} + \frac{1}{2\Gamma_L - i\omega_{\alpha\beta}}\frac{1}{\Gamma_L - i(\omega_L-\omega_{\beta n})} + \frac{1}{2\Gamma_L - i\omega_{\alpha\beta}}\frac{1}{\Gamma_L - i(\omega_L-\omega_{\alpha n})}\right\} + CC \tag{15}$$

$$W_{\alpha\beta}(\omega_0) = \sum_n V_{\alpha n}V_{n\beta}\left\{\frac{1}{\Gamma - i(\omega_0-\omega_{\alpha n})}\frac{1}{\Gamma+\gamma - i(\omega_0-\omega_{\beta n})} + \frac{1}{2\Gamma+\gamma - i\omega_{\alpha\beta}}\frac{1}{\Gamma+\gamma - i(\omega_0-\omega_{\beta n})} + \frac{1}{2\Gamma+\gamma - i\omega_{\alpha\beta}}\frac{1}{\Gamma - i(\omega_0-\omega_{\alpha n})}\right\} + CC \tag{16}$$

Here $V_{\alpha n}$ and $V_{n\beta}$ are the matrix elements of the transition dipole moments between the eigenstates $|\alpha\rangle$ and $|\beta\rangle$ (belonging to the excited electronic state) and $|n\rangle$ (belonging to the ground electronic state). These are the final expressions for the TFG SE spectrum which are used in all subsequent calculations.

3. ET Model

The standard model of an ET system consists of a ground state and two electronically coupled excited donor and acceptor states.[51] The excited states are linearly coupled to a reaction mode (Figure 1), which in turn is weakly coupled to a harmonic bath. In the present context, the general formula (5) is specialized as follows: the electronic states and vibrational modes, which are directly involved in the reaction, constitute the relevant system and are described by H^S. The bath degrees of freedom (described by H^B) are only indirectly involved via the system-bath coupling H^{SB}, which is assumed to be weaker than the primary interactions contained in the system Hamiltonian.

We shall restrict ourselves to the consideration of a single-vibrational-mode system Hamiltonian

$$H_g^S = |g\rangle\, H_0\, \langle g| \tag{17}$$

$$H_0 = \Omega\{b^\dagger b + 1/2\} \tag{18}$$

$$H_e^S = \sum_{i=1,2} |\phi_i\rangle\, (H_i + \epsilon_i^0)\, \langle\phi_i| + \{|\phi_1\rangle\, V_{12}\, \langle\phi_2| + HC\} \tag{19}$$

$$H_i = \Omega\left\{b^\dagger b + 1/2 - \frac{\Delta_i}{2^{1/2}}(b^\dagger + b)\right\} \tag{20}$$

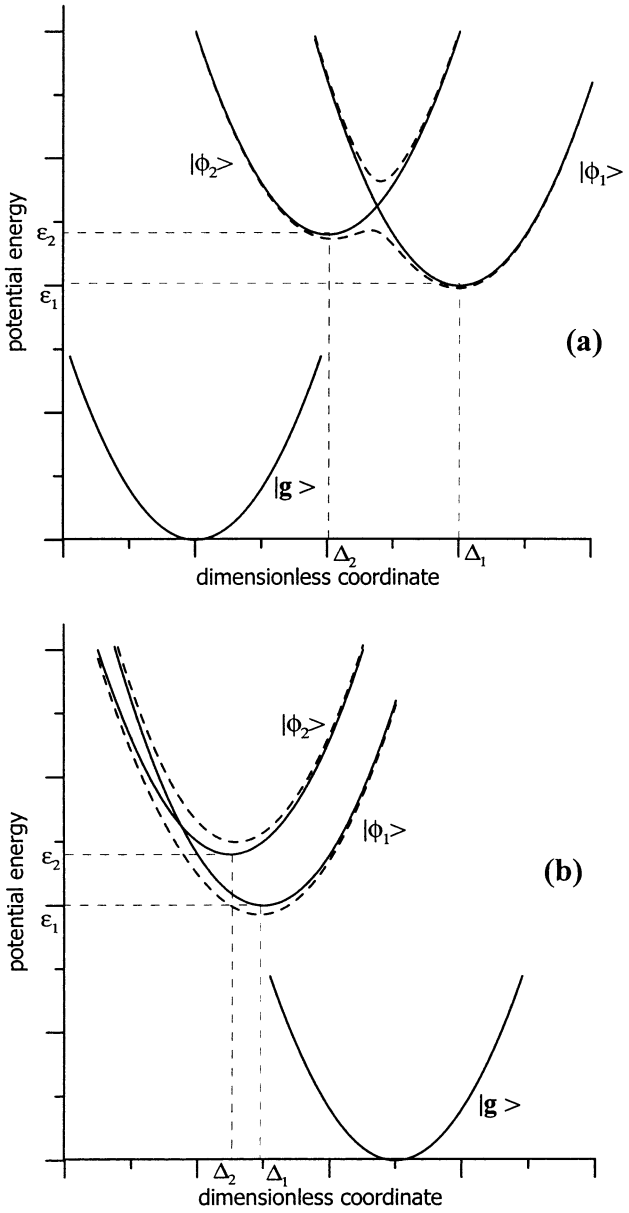

Figure 1. Diabatic (solid) and adiabatic (dashed) potential-energy surfaces for the normal (a) and inverted (b) regime.

Here $|\phi_2\rangle$ and $|\phi_1\rangle$ label the diabatic donor and acceptor excited electronic states, ϵ_i^0 are the vertical electronic excitation energies, the vertical displacements (0−0 transition energy) are given by (see Figure 1): $\epsilon_i = \epsilon_i^0 - \Omega\Delta_i^2/2$, and V_{12} is the electronic coupling matrix element (V_{12} should not be confused with the matrix elements of the transition dipole moments $V_{\alpha n}$ and $V_{n\beta}$ in eqs 15, 16). The vibrational Hamiltonians, which are written in the second quantization representation, are taken to be harmonic. Ω is the vibrational frequency of this reaction mode (it is assumed to be the same for both electronic states) and Δ_i are the horizontal displacements of the excited-state potentials from the energy minimum of the electronic ground state. It is assumed that the ET takes place between the two excited electronic states, one of which (the donor state $|\phi_2\rangle$) is optically bright, while the second (the acceptor state $|\phi_1\rangle$) is optically dark, so that the transition-dipole operator is $V_{\text{eg}} \sim |g\rangle\langle\phi_2| + \text{HC}$.

A standard assumption is to model the bath by a collection of harmonic oscillators:

$$H^{\text{B}} = \sum_q \omega_q (a_q^{\dagger} a_q + 1/2) \tag{21}$$

We further introduce the simplest approximation for the system-bath interaction, a bilinear system−bath coupling in the rotating-wave approximation[52,53]

$$H^{\text{SB}} = \sum_q g_q (b^{\dagger} a_q + b a_q^{\dagger}) \tag{22}$$

The system-bath coupling is assumed to be the same for both electronic states. It is entirely described by the so-called bath spectral function $J(\omega)$. The latter has been taken in the Ohmic form with exponential cutoff,[54] viz.

$$J(\omega) = \eta\omega \exp\{-\omega/\omega_{\text{c}}\} \tag{23}$$

Here η is a dimensionless system-bath coupling strength and ω_{c} is a cutoff frequency.

As has been mentioned earlier, the key quantity describing the relevant system dynamics is the RDM (6), which is defined as the trace over all bath variables of the full density matrix. In the present article, the RDM $\sigma(t_0)$ is calculated in the framework of Redfield theory, as has been described in detail elsewhere.[55] Assuming sufficiently weak system-bath coupling, the bath degrees of freedom are traced out in the Born and Markov approximations, yielding the Redfield equation of motion for the RDM in the system eigenstate representation,[56,57] so that eq 6 is written explicitly as follows

$$\frac{\partial \sigma_{\mu\nu}(t)}{\partial t} = -i\omega_{\mu\nu}\sigma_{\mu\nu}(t) + \sum_{\kappa\lambda} R_{\mu\nu\kappa\lambda}\sigma_{\kappa\lambda}(t) \tag{24}$$

Here $R_{\kappa\lambda\mu\nu}$ is the relaxation or Redfield tensor. The first term on the right-hand side describes the isolated system evolution, while the second one represents its interaction with the dissipative environment. The Redfield tensor, which is responsible for the system relaxation, can be expressed as

$$R_{\mu\nu\kappa\lambda} = \Gamma^{+}_{\lambda\nu\mu\kappa} + \Gamma^{-}_{\lambda\nu\mu\kappa} - \delta_{\nu\lambda}\sum_{\alpha}\Gamma^{+}_{\mu\alpha\alpha\kappa} - \delta_{\mu\kappa}\sum_{\alpha}\Gamma^{-}_{\lambda\alpha\alpha\nu} \tag{25}$$

where

$$\Gamma^{+}_{\lambda\nu\mu\kappa} = \int_0^{\infty} \mathrm{d}t\, \langle\langle\lambda|H^{\text{SB}}(t)|\nu\rangle\langle\mu|H^{\text{SB}}|\kappa\rangle\rangle_{\text{B}}\, \mathrm{e}^{-i\omega_{\mu\kappa}t} \tag{26}$$

$$\Gamma^{-}_{\lambda\nu\mu\kappa} = \int_0^{\infty} \mathrm{d}t\, \langle\langle\lambda|H^{\text{SB}}|\nu\rangle\langle\mu|H^{\text{SB}}(t)|\kappa\rangle\rangle_{\text{B}}\, \mathrm{e}^{-i\omega_{\lambda\nu}t} \tag{27}$$

$$H^{\text{SB}}(t) = \mathrm{e}^{iH^{\text{B}}t} H^{\text{SB}}\, \mathrm{e}^{-iH^{\text{B}}t} \tag{28}$$

and $\langle\ldots\rangle_{\text{B}}$ denotes the thermal average over the bath. For the Hamiltonians defined above, the Redfield tensor components can be expressed in closed form.[26,55]

Equations 24−28 (Redfield equations of motion) together with eqs 14−16 (TFG SE spectrum) are utilized to calculate TFG SE signals for the ET system. The basic scheme for the calculations is the following: The first step is to evaluate the system eigenstates (eq 12). One then calculates the D function (15) which describes the optically prepared initial state of the system

$$\sigma_{\alpha\beta}(0) = D_{\alpha\beta}(\omega_{\text{L}}) \tag{29}$$

After that one performs a propagation over a time interval t_0 according to the Redfield equations (24−28) with the initial

condition (29), yielding the RDM $\sigma_{\alpha\beta}(t_0)$. For nontrivial systems, this is the computationally most expensive part. In the present article, a fourth-order Runge−Kutta scheme[58] has been employed for the numerical time propagation. The final step is the contraction of the RDM $\sigma(t_0)$ with the W function (16) which describes the detection process. This yields the desired TFG SE spectrum

$$S_{st}(t_0,\omega_0) = \sum_{\alpha,\beta} W_{\alpha\beta}(\omega_0)\, \sigma_{\alpha\beta}(t_0) \tag{30}$$

It should be remarked that for electronically nonadiabatic systems the use of the eigenstate representation is computationally feasible for system Hamiltonians containing several vibrational modes (up to seven in favorable cases[19]), so that the use of eqs 12 is not very restrictive. Note that this method requires the D and W operators to be calculated only once.

4. TFG SE Spectra of ET Systems: Specific Examples and Discussion

To reveal the connection between the electronic population dynamics and spectroscopic measurements, we consider the frequency-integrated signal

$$I(t_0) = \int_{-\infty}^{\infty} \mathrm{d}\omega_0\, S_{st}(t_0,\omega_0) = Tr\{\tilde{W}\sigma(t_0)\} \tag{31}$$

where

$$\tilde{W} = \int_{-\infty}^{\infty} \mathrm{d}\omega_0\, W(\omega_0) \tag{32}$$

is the frequency-integrated W operator. Evidently, the integral signal is equivalent to the TFG SE signal in the limit of poor frequency resolution ($\gamma \to \infty$).[49] In terms of the system eigenstates[50]

$$\tilde{W}_{\alpha\beta} \sim \langle\alpha|\phi_2\rangle\langle\phi_2|\beta\rangle \frac{4\Gamma^2}{4\Gamma^2 + \omega_{\alpha\beta}^2} = \sum_n V_{\alpha n} V_{n\beta} \frac{4\Gamma^2}{4\Gamma^2 + \omega_{\alpha\beta}^2} \tag{33}$$

It is further useful to consider separately the limiting cases of good ($\Gamma \to \infty$) and poor ($\Gamma \to 0$) temporal resolution. If the gate pulses are short enough ($\Gamma \to \infty$), then $\tilde{W} = |\phi_2\rangle\langle\phi_2|$ and

$$I(t_0) = \sum_{\alpha,\beta} \sigma_{\alpha\beta}(t_0)\langle\alpha|\phi_2\rangle\langle\phi_2|\beta\rangle = Tr[|\phi_2\rangle\langle\phi_2|\,\sigma(t_0)] = P_2(t_0) \tag{34}$$

The integral signal is thus nothing else than the time-dependent population $P_2(t_0)$ of the diabatic donor state $|\phi_2\rangle$. The fact that in the ideal limit of ultrashort pulses the integral fluorescence signal is equivalent to the diabatic population of the optically bright electronic state has been established earlier by Meyer and Koeppel[59] and for the integral pump−probe signal by Domcke and Stock.[60,61]

If the gate pulses are longer than any relevant time scale of the system dynamics ($\Gamma \to 0$), then

$$\frac{4\Gamma^2}{4\Gamma^2+\omega^2_{\alpha\beta}} = \delta_{\alpha\beta} \tag{35}$$

so that

$$I(t_0) = \sum_{\alpha} \sigma_{\alpha\alpha}(t_0)\langle\alpha|\phi_2\rangle^2 \tag{36}$$

In the system-eigenstate representation, the difference between these two limits becomes transparent. For poor temporal resolution ($\Gamma = 0$), the signal is simply the weighted sum of populations $\sigma_{\alpha\alpha}$ (see eq 36), while the perfectly time-resolved signal contains the contributions from both coherences $\sigma_{\alpha\beta}$ ($\alpha \neq \beta$) and populations $\sigma_{\alpha\alpha}$ (see eq 34). Thus, the comparison of the signals for good and poor temporal resolution allows one to reveal the importance of coherences in the RDM.

When there is no coupling between the excited electronic states (and thus no ET), the integral signal is simply proportional to the constant (time-independent) population of the bright state, irrespective of the time resolution.[60] The nonadiabatic coupling is therefore responsible for the time dependence of the population and the evolution of the integral optical signal. Alternatively, non-Condon effects in adiabatic systems also result in a time dependence of the integral fluorescence signal.[4,60,62]

To learn about the interrelation between the integral signal and the population dynamics, we present below the results of explicit calculations. The system-bath interaction is described by the spectral function (23) with $\omega_c = \Omega$. The bath is assumed to be in equilibrium at zero temperature to emphasize quantum tunneling effects. We begin with the consideration of the effect of temporal resolution. To render the presentation more transparent, we separate the influence of the gate-pulse duration from that of the pump pulse, restricting ourselves initially to the case of impulsive excitation. In other words, the system is instantaneously excited from the ground electronic state to the donor ($|\phi_2\rangle$) electronic state. The preparation is referred to as stationary, if there is no shift between the equilibrium configurations of the ground and excited electronic states, and as nonstationary otherwise.

4.1. Electronic Coherence in ET. We start from the consideration of an ET system in the so-called normal regime (Figure 1a). The system parameters have been taken from:[26] $\Omega = 0.05$ eV, $\Delta_1 = 3.5$, $\Delta_2 = 0$ (stationary preparation), $\epsilon_0 = 0$ eV, $\epsilon_1 = 1.455$ eV, $\epsilon_2 = 1.5$ eV (the minimum of the potential surface for the donor state is higher than that for the acceptor state), and $V_{12} = \Omega$ (strong electronic coupling). The coupling to the bath is assumed to be rather weak ($\eta = 0.1$).

The donor-state population dynamics for this system is given by curve 1 in Figure 2a. This particular system (stationary preparation and strong electronic coupling) is a good example for the observation of EC in the ET reaction. Since no horizontal shift is assumed between the minima of the $|g\rangle$ and $|\phi_2\rangle$ energy surfaces, the vibrational effects (in particular, VC) are of minor importance. The large-amplitude quantum beatings in the population dynamics reflect the presence of EC. Indeed, sufficiently large values of electronic coupling can result in coherent electronic motion ("coherent ET") between the donor and acceptor electronic states. These beatings are analogous to the well-known Rabi oscillations in optical physics.

The fast oscillations in curve 1 of Figure 2a arise from the peculiarities of the initial preparation. Indeed, the WP is put at $t_0 = 0$ into the unperturbed ($V_{12} = 0$) ground vibrational state of $|\phi_2\rangle$. However, because of the strong electronic coupling, this initial vibrational state deviates significantly from the eigenstates of the distorted adiabatic potential.

Figure 2a shows the integral signals calculated for this system, assuming four different time resolutions, varying from good ($\Gamma = 2\Omega$) to poor ($\Gamma = \Omega/100$). The assumption that the pulses are short compared with the time scale of system-bath relaxation (cf. the derivation of eqs 7−9) is well fulfilled, except the last case ($\Gamma = \Omega/100$). In this case, strictly speaking, this assumption is not valid, and the theory may not be quantitatively accurate,

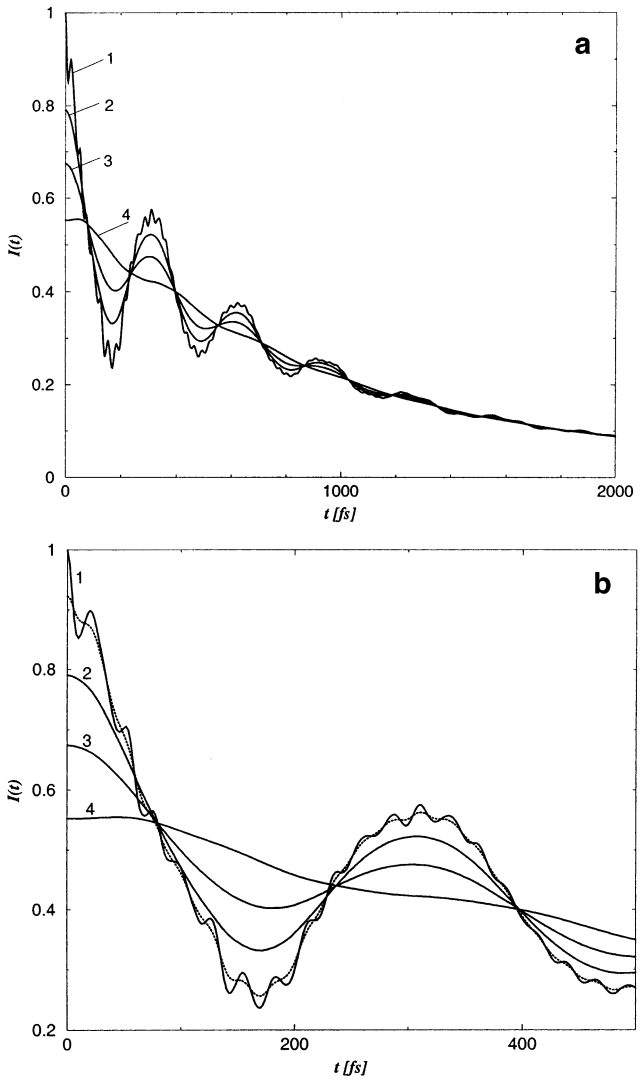

Figure 2. (a) Influence of the temporal resolution on the integral SE signal of a model ET system (normal regime, stationary preparation, strong electronic coupling) exhibiting EC: 1, $\Gamma > 2\Omega$ (population dynamics); 2, $\Gamma = \Omega/5$; 3, $\Gamma = \Omega/10$; 4, $\Gamma = \Omega/100$. (b) Same as in Figure 2a, but for the first 500 fs. The additional dotted line corresponds to $\Gamma = \Omega$.

but the results should reflect the qualitative effect in this limit (poor time resolution). The calculations show that for good temporal resolution (up to $\Gamma = 2\Omega$) the integral signal follows the diabatic population of the donor state. In Figure 2a, the corresponding kinetics are undistinguishable from that given by curve 1: they reproduce all the features of the population dynamics, even the fast oscillations of vibrational origin. The equivalence of integral signal and population dynamics is a direct consequence of the theoretical analysis discussed above.

With decreasing Γ, the integral signal becomes smoother, but, as expected, the electronic beatings are seen in curves 2 and 3 in Figure 2a ($\Gamma = \Omega/5$ and $\Gamma = \Omega/10$, respectively). Finally, when we take really poor time resolution (curve 4, $\Gamma = \Omega/100$), which corresponds to a gate pulse which is much longer than the time scale of EC, we loose the electronic beatings in the signal. For such long gate pulses, the time resolution becomes inadequate to resolve the quantum beats in the population dynamics. It is noteworthy that the smoothing of integral signal with decreasing temporal resolution looks like a time-averaging process: all the curves in Figure 2a pass through the same intersection points. For poor resolution ($1/\Gamma$ larger than the time scale of EC), the fast system dynamics cannot be resolved and one measures only the time-averaged signal, describing the rate process of the population decay from the donor to acceptor state.

Clearly, the temporal resolution $\Gamma = \Omega$ (when the gate pulse is of the order of the vibrational period) is critical for the observation of the fast-oscillating vibrational structure, originating from the peculiarities of the initial preparation. The corresponding signal is given by the dotted line in Figure 2b, which shows in detail the early-time part (first 500 fs) of the population dynamics and fluorescence signals presented in Figure 2a. When $\Gamma = \Omega$, the vibrational oscillations in the integral signal disappear, but the signal still exhibits the same electronic oscillations as in the case of high temporal resolution. Although the value of the electronic coupling is equal to the vibrational frequency in this example, the period of these electronic beatings is much longer than $1/\Omega$. The explanation of this seemingly puzzling fact is simple: $V_{12} = \Omega$ does not mean that the characteristic time scale of the EC is of the order of $1/\Omega$. The frequency of the electronic quantum beats is rather determined by the electronic coupling matrix element, renormalized by the Franck−Condon overlap integral of the relevant vibrational wave functions of the diabatic potentials. One can estimate this time scale from Figure 2 as ~400 fs. Taking into account that the vibrational period corresponding to $\Omega = 0.05$ eV is $T_{vib} = 83$ fs, one can expect that electronic oscillations in the integral signal can be seen up to values $\Gamma \sim \Omega/5$. This conclusion is confirmed by the results of our calculations (see Figure 2a).

This example gives a clear confirmation of our qualitative considerations on the integral signal (see discussion above). In Figure 2a, the signal corresponding to good resolution (curve 1) shows contributions from both populations and coherences, while in the case of poor time resolution, the coherences are no longer present in the signal which simply reflects monotonic population decay. All curves have the same long-time decay, giving the ET rate which is independent of temporal resolution. As expected, the difference between the highly and poorly time-resolved signals is important on short time scales (when coherences are not yet destroyed). For instance, with decreasing time resolution the absolute value of the integral signal at $t = 0$ is significantly less than 1.

The discussed model system is a good example for the observation of EC in ET. We conclude that the very existence of electronic beatings for the present ET system can be observed with gate pulses as long as $1/\Gamma = 10/\Omega \approx 830$ fs. Therefore it seems that the temporal resolution is not a critical parameter for the observation of EC; the necessary temporal resolution can be easily achieved with pulses available nowadays. Nevertheless, to the knowledge of the authors, electronic population oscillations of the type shown in Figure 2a have not yet been observed in real systems. The quantum beats observed so far in femtosecond time-resolved pump−probe and fluorescence signals for numerous ET systems appear to be of vibrational origin.[3,34] An experiment which was especially designed to detect EC in ET has failed.[32] In real systems, extremely short (of the order of several femtoseconds) dephasing times are the most important obstacle for the observation of the EC. In the ET model system discussed here, the dephasing time was long enough to allow the observation of EC at a time scale of the order of 1 ps.

There might be another possible reason for the failure of the above-mentioned attempt to detect EC in ET. The amplitude of the EC effect is extremely sensitive to the choice of system parameters, especially the initial preparation and the electronic

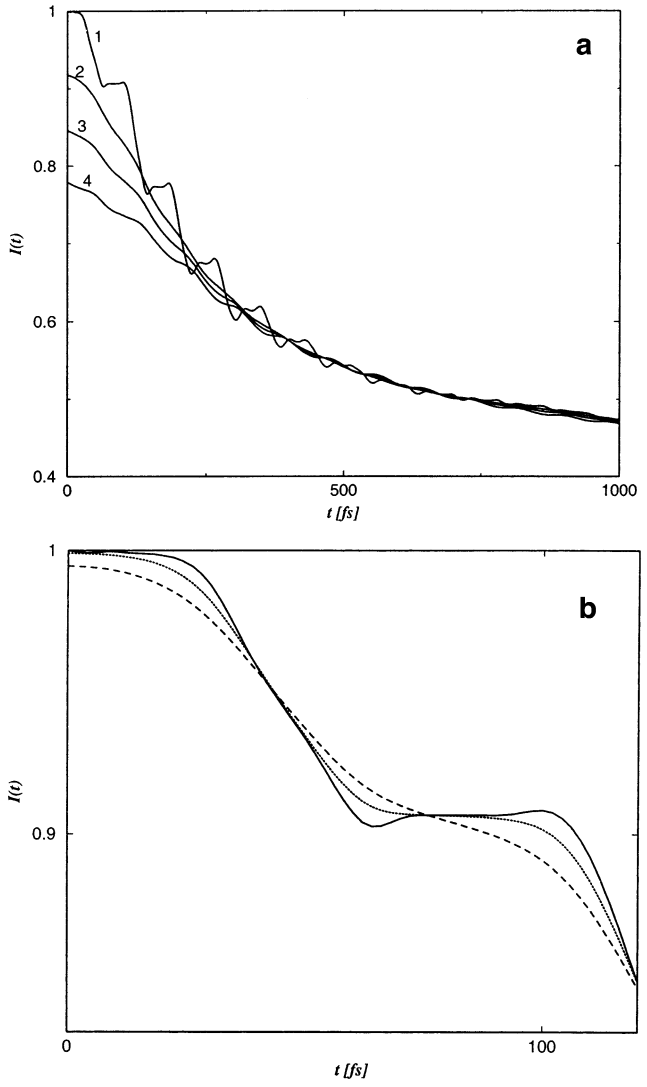

Figure 3. (a) Influence of temporal resolution on the integral SE signal of a model ET system (normal regime, nonstationary preparation, weak electronic coupling) exhibiting VC: 1, $\Gamma > 2\Omega$ (population dynamics); 2, $\Gamma = \Omega/10$; 3, $\Gamma = \Omega/20$; 4, $\Gamma = \Omega/50$. (b) Same as in Figure 3a, but for the first 130 fs: solid line, $\Gamma > 2\Omega$; dotted line, $\Gamma = \Omega$; dashed line, $\Gamma = \Omega/2$.

coupling strength. It is therefore not unlikely that for a particular molecule and for a particular configuration of experiment, EC effects are not present at all.

4.2. Vibrational Coherence in ET. Next we consider again an ET system in the normal regime (Figure 1a), but two important system parameters are taken different from the previous case: $V_{12} = \Omega/5$(weak electronic coupling) and $\Delta_1 = 5.5$, $\Delta_2 = 2$.[26] This choice corresponds to nonstationary preparation, that is, there is a shift between the equilibrium configurations of the ground and donor electronic states. Due to the weak electronic coupling, the EC is strongly suppressed, but a new effect, VC, shows up as a consequence of the nonstationary preparation. The instantaneous excitation results in the preparation of a WP in the excited electronic state which subsequently performs coherent vibrational motion. As can be seen from Figure 1a, the mean energy of the initial wave packet lies above the energy of the crossing point of the diabatic potentials, that is, the crossing point is accessible for the moving wave packet.

The population dynamics for this system calculated via Redfield theory is given by curve 1 in Figure 3a. It exhibits a peculiar and easily interpretable behavior, reflecting the combined effect of vibrational WP dynamics in the donor state and ET, namely, a steplike decay of donor-state diabatic population $P_2(t_0)$. Obviously, due to the presence of electronic coupling, a fraction of the WP is transferred to the acceptor state each time the moving WP hits the crossing region (at $t_0 = 2\pi n/\Omega$, $n = 1$, 2, ...). The characteristic stepwise structure thus reflects this ultrafast ET process driven by coherent WP motion, which is quenched after ~500 fs due to vibrational damping. After the WP motion is relaxed, the donor-state population exhibits a monotonic decay, analogous to the long-time decay in the case of stationary preparation in Figure 2. Similar steplike population behaviors at short times and bimodal decay curves have been obtained by several authors[21,63−65] and also observed experimentally.[4,35] These features appear to be generic for ultrafast ET dynamics with nonstationary preparation for systems with a single or few system vibrational modes.

Now we proceed to the discussion of the integral signals calculated for this system with different time resolutions, ranging from good ($\Gamma = 2\Omega$) to poor $\Gamma = \Omega/50$). Figure 3a shows the overall behavior, while Figure 3b gives a detailed picture of the short-time dynamics. The main point is the criterion for the observation of the characteristic steps in the integral signal. Qualitatively, the influence of the time resolution is very similar to that established in the previous case (Figure 2). For good temporal resolution (up to $\Gamma = 2\Omega$), the integral signal coincides with the population dynamics (curve 1 in Figure 3a and solid line in Figure 3b); the time resolution $\Gamma = \Omega$ (dotted line in Figure 3b) is at the borderline for the observation of steps; for slightly worse temporal resolution (dashed line in Figure 3b, corresponding to $\Gamma = \Omega/2$) the steps are washed out in the integral signal. If one further decreases the temporal resolution (curves 2−4 in Figure 3a, corresponding to the temporal resolution $\Gamma = \Omega/10$, $\Gamma = \Omega/20$, and $\Gamma = \Omega/50$, respectively) the gate pulse averages out all characteristic features of the system dynamics, resulting in a smooth decay curve. The rate of the long-time exponential decay is independent of the temporal resolution. On the contrary, the short time (up to 500 fs) behavior of the signals depends significantly on the time resolution, because the coherences are not yet destroyed. In contrast to the EC, the time scale of the VC is determined by the system vibrational period, $T_{vib} = 83$ fs. Thus the time scale of the VC is much shorter than that of the EC (~400 fs) in our system. Therefore the characteristic features of VC disappear faster with decreasing time resolution than in the previous case. For example, a time resolution $\Gamma = \Omega/10$ is still enough to observe the EC (Figure 2), while for the VC (Figure 3) this is already beyond the limit of resolution.

4.3. TFG SE Spectra. Experimentally, a TFG SE spectrum can be constructed from the data for a range of times between the excitation pulse and the gate pulse, and a range of frequency windows determined by the spectral filter. In this section we present 3D TFG spectra calculated using eq 30 for the systems considered in detail in a previous section. To primarily concentrate on the dynamic effects, a perfect time ($\Gamma = 10\Omega$) and frequency ($\gamma = \Omega/20$) resolution has been chosen for all calculations.

The TFG SE spectrum for the ET system with EC (system considered in section 4.1) is presented in Figure 4. The spectrum, as a function of time, qualitatively reflects the electronic population dynamics: one can clearly see the large-amplitude electronic beatings mirroring coherent ET as well as the fast oscillations due to peculiarities of the initial preparation. Cuts

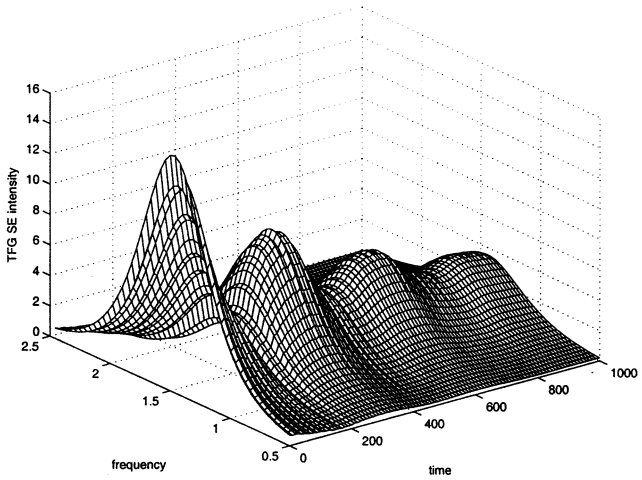

Figure 4. TFG SE spectrum of the ET system exhibiting EC in the case of good time and frequency resolution.

of the spectrum at fixed frequencies, i.e., the transients which are usually measured experimentally, in general, have very different behavior. For example, the cut at the frequency close to 0−0 transition reproduces the population dynamics almost quantitatively, while the cuts at the wings of the spectrum give a qualitatively different behavior (compare with refs 60 and 61). Therefore, the problem of a theoretical reproduction of experimental 3D TFG SE spectra is quite demanding, because one must achieve a coincidence for all particular frequency cuts. In turn, this imposes restrictions on the choice of system parameters. Ideally, this would help one to fit the system parameters in a unique way.

As a function of frequency, on the other hand, the TFG spectrum at $t_0 = 0$ represents the SE of the initially prepared nonequilibrium excited state. Later on, at every time moment t_0, it represents the time evolution of the fluorescence spectrum. The area under the instantaneous spectra $S(\omega_0,t_0)$ decreases with time, reflecting the decay of the population in the donor electronic state. In the limit $t_0 \rightarrow \infty$, the TFG SE spectrum is nothing else than the relaxed fluorescence spectrum.[49] For the ET system under consideration, the donor state population tends toward zero for $t_0 \rightarrow \infty$; therefore, there is no relaxed fluorescence.

The TFG SE spectrum for the ET model with VC (system considered in section 4.2) is depicted in Figure 5a. Again, the time evolution of the signal monitors the ET dynamics: we can see the steps occurring in the donor-state population. In addition, the signal, as a function of frequency, maps directly the periodic vibrational WP motion in the excited state. To show this explicitly, the TFG SE signal is displayed in Figure 5b during the first two periods. The time evolution of the spectrum within each step reminds us of that of the Brownian oscillator.[45,49] The WP exhibits quasiperiodic behavior, moving between classical turning points, where the local maxima of the peak shift occur. If the temporal and spectral resolutions are good enough, the intensity and the shape of the spectrum do not change within each step (compare with Figure 1c in ref 49, where the TFG spectrum is given for a Brownian oscillator). Every time the WP comes to the crossing point of the two diabatic potentials, part of it leaks to the acceptor state, producing a step in the electronic population. Thus, the crossing point can indeed be regarded as a "sink", as it is assumed in Zusman-type models of ET.[66] This picture does not apply, on the other hand, to the description of the dynamics of the ET system with EC (Figures 2 and 4), because the population

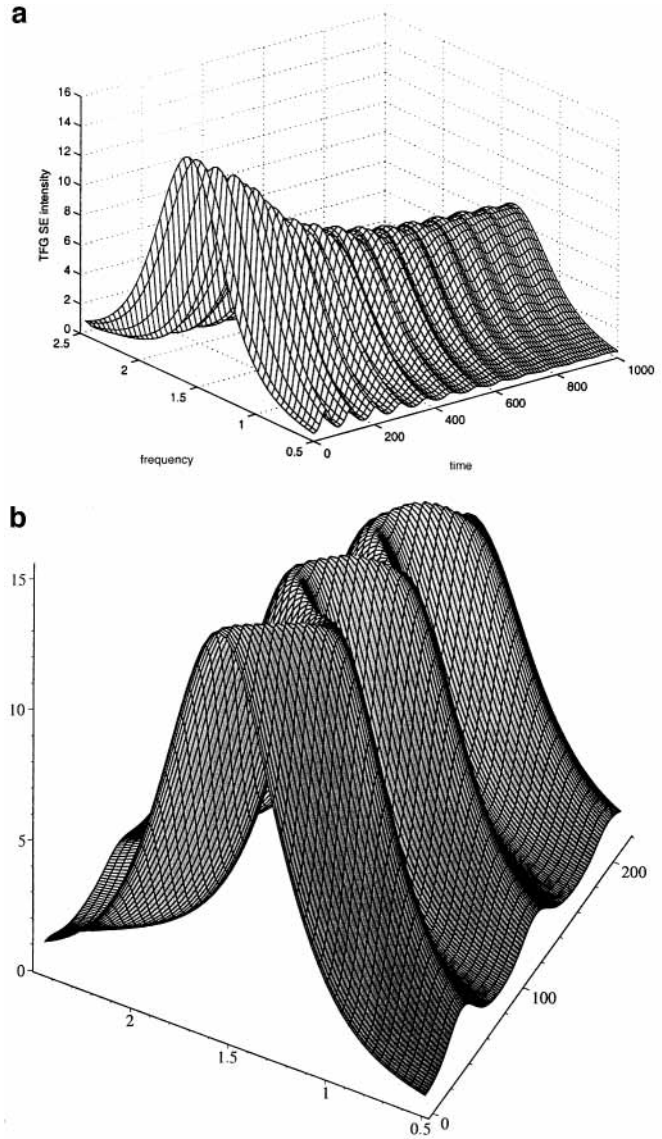

Figure 5. (a) TFG SE spectrum of the ET system exhibiting VC in the case of good time and frequency resolution. (b) Same as in Figure 5a, but for the first two vibrational periods (∼200 fs).

dynamics in that case is not monotonic, but quasiperiodic, and cannot be described by an effective "sink".

Summarizing, both electronic and vibrational coherences contribute to the population dynamics for ultrafast ET systems. If short enough pulses are employed, both types of coherences manifest themselves in the measured TFG SE spectra. Moreover, TFG SE spectra provide us with more information on the system dynamics than frequency-averaged time-resolved signals or the conventional stationary fluorescence spectrum. In fact, the TFG SE signal $S(\omega_0,t_0)$ gives the actual spectral shape (e.g., Gaussian, Lorentzian, or more complicated) and shows directly the evolution of the fluorescence spectrum with time. It is thus very useful for a detailed understanding of the system dynamics.

4.4. Finite Pump Duration. Finally, we study briefly another aspect of ultrafast time-resolved spectroscopy: the effect of the system preparation by a pump pulse of finite duration. Evidently, the amount of vibrational energy and coherence initially deposited into the system is determined by the temporal and spectral properties of the excitation pulse. To separate the effect of the pump-pulse duration from that of the time-gate duration considered in section 4.1, a good temporal resolution of the gate pulse ($\Gamma = 2\Omega$) is assumed in the following.

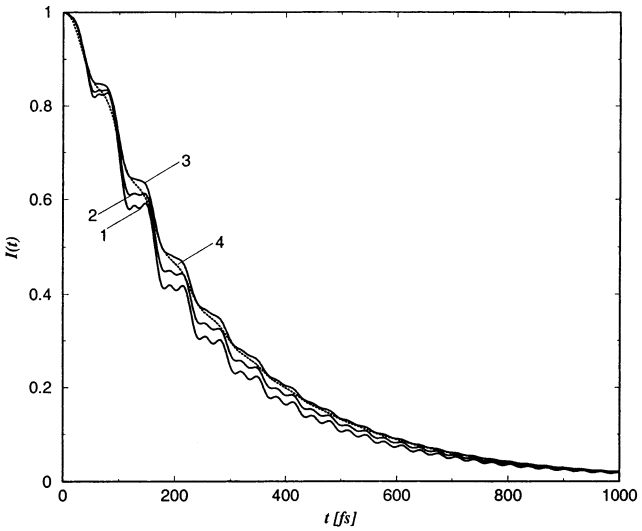

Figure 6. Influence of pump-pulse duration on the integral SE signal of a ET system in the inverted regime: 1, $\Gamma_L = 10\Omega$; 2, $\Gamma_L = 3\Omega$; 3, $\Gamma_L = \Omega$; 4 (dotted line), $\Gamma_L = \Omega/10$.

To analyze different scenarios of ultrafast ET within the present model, we consider a system in the so-called inverted regime. The potential-energy surfaces are given in Figure 1b, and the system parameters are taken as follows:[26] $\Omega = 0.064$ eV, $\Delta_1 = -0.8281$, $\Delta_2 = -2$, $V_{12} = 0.1$ eV, and $\epsilon_0 = 0$ eV, $\epsilon_1 = 2.8741$ eV, $\epsilon_2 = 3$ eV, $\eta = 0.4219$.

The integral signals calculated for this ET system prepared by pump pulses of different duration are plotted in Figure 6. The pump pulse is described by eq 10, so that the time-integrated intensity is kept fixed when the pulse duration is varied. The signals, on the other hand, are normalized to unity at $t_0 = 0$, i.e., $I(0) = 1$. The problem of normalization deserves further clarification. If one considers unnormalized signals calculated according to eq 31, one finds that the shorter the pump pulse, the larger is the absolute value of the signal. (This fact was well-established earlier for the pump−probe spectroscopy.[19]) Indeed, short pump pulses have a broad bandwidth and can excite coherently many vibrational levels, so that ET occurs from a number of initially excited levels. A long pump pulse, on the other hand, excites only a few vibrational levels, which results in a significant decrease of the absolute value of the integral signal. This must be contrasted to the time-resolution effect of the gate (Figure 2). In that case, the smaller initial values of $I(t_0)$ are the result of the detection procedure: long gate pulses average over the population dynamics.

Keeping this in mind, we are in a position to analyze the dependence of the integral signal on the duration of the pump pulse (see Figure 6). The effect of pump-pulse duration qualitatively looks very similar to the effect of time resolution of the gate: the steplike structure reflecting WP motion can be well detected with short pump pulses (curves 1 and 2, which correspond to $\Gamma_L = 10\Omega$ and $\Gamma_L = 3\Omega$, respectively). The pump-pulse duration of the order of the vibrational period (curve 3, $\Gamma_L = \Omega$) is the critical one: the characteristic effects of coherent vibrational motion are nearly wiped out in the integral signal. For longer pump pulses (curve 4, $\Gamma_L = \Omega/10$), the system is prepared in such a way that no features of vibrational coherence can be detected, although the time resolution of the gate is sufficient to detect them.

To monitor the microscopic features of the ET dynamics in a TFG SE experiment, one must thus employ sufficiently short pump pulses to excite coherently a significant part of the vibrational levels. What is less intuitive, the structures of the integral signal are as sensitive to the pump-pulse duration as to the gate-pulse duration. To detect the mode-specific steplike structure in ultrafast spectroscopic signals of ET process, the pump-pulse duration as well as the gate-pulse duration must be shorter than the vibrational period.

5. Conclusions

We have presented the application of the theory of TFG SE signals to nontrivial examples: ultrafast ET processes. The TFG as well as frequency-integrated SE signals have been calculated for various durations of the pump and gate pulse. Our main findings can be summarized as follows.

The integral signal obtained with sufficiently short gate pulses (i.e., good temporal resolution) reflects most directly the donor-state diabatic population. If the temporal resolution decreases, system-specific features are wiped out, and the signal simply reflects monotonic decay of the population of the donor state. In the system eigenstate representation, the difference between these two limits becomes transparent. For poor time resolution, the signal is simply the weighted sum of populations $\sigma_{\alpha\alpha}$ (eq 36), while the perfectly resolved signal contains the contributions from both coherences $\sigma_{\alpha\beta}$ ($\alpha \neq \beta$) and populations $\sigma_{\alpha\alpha}$ (eq 34). Thus the comparison of the signals obtained with good and poor temporal resolution allows one to estimate the importance of coherence effects in the system dynamics. The difference between the two limits is pronounced on short time scales (when coherences are not yet destroyed). The rate of the long-time decay (ET rate) is independent of the temporal resolution.

The effect of optical preparation by pump pulses of finite duration is qualitatively similar to that of temporal resolution of the gate pulse. To monitor the mode-specific features of the ET dynamics in a TFG SE experiment, one must employ sufficiently short pump pulses to excite coherently a significant part of vibrational levels. To detect the characteristic steplike structure in ultrafast spectroscopic signals, the pump-pulse duration as well as the gate-pulse duration must be shorter than the vibrational period.

To elucidate the effect of various coherences on SE signals, we have performed simulations for ET models in which either EC or VC effects are dominant. For the observation of electronic quantum beats, the time resolution of the gate must be of the order of or shorter than the electronic beating period. Provided the time-gate duration is of the order of a vibrational period or shorter, VCs were shown to manifest themselves through the characteristic steplike structures in the electronic population. It should be noted that the prediction of such peculiar steplike structures is not limited to the case of weak system-bath coupling, which is described by Redfield theory. They manifest themselves in the population dynamics also in calculations carried out beyond this limit.[65,67,68]

Both types of coherences can show up in measured TFG SE spectra. The TFG SE spectrum $S(\omega_0, t_0)$ as a function of time qualitatively reflects the electronic population dynamics: either electronic beatings reflecting EC or the steps occurring in the donor-state population due to VC. In addition, the frequency-dependent TFG spectrum at $t_0 = 0$ represents the SE of the initially prepared nonequilibrium excited state. Later on, at every time moment t_0 it gives the development of this fluorescence spectrum. Most importantly, the time- and frequency-resolved signal maps directly the periodic vibrational WP motion in the excited state. TFG SE spectra provide us therefore with more information on the system dynamics than frequency-averaged time-resolved signals or the conventional stationary fluorescence spectrum.

To summarize, the influence of the measuring devices (the pump pulse for preparation and the gate pulse for detection) is significant and must be accurately taken into account. The presented results illustrate the relation between the "pure" (intrinsic) dynamics of ET systems (e.g., the time-dependent electronic population dynamics) and "real" experimental observables. This aspect is new in comparison with the investigations of Jean.[36] We hope that the methods developed in the present work may prove useful for the interpretation of TFG SE experiments on ultrafast ET systems exhibiting coherent responses. The present approach can be directly applied to the description of experiments which detect ultrafast ET processes via time-gated fluorescence for systems which are described by three-state ET models (i.e., with a separate electronic ground state). In this context, the experiments of Yoshihara and coworkers on the electron donor−acceptor complex TCNE−HMB and related systems are of particular interest.[4] Work in this direction is in progress.

Acknowledgment. We are grateful to Michael Thoss for fruitful discussions and to Dassia Egorova for providing the Redfield propagation code. This work has been supported by the Deutsche Forschungsgemeinschaft through SFB 377. M.F.G. acknowledges financial support through a visitor grant.

References and Notes

(1) Steinmeyer, G.; Sutter, D. H.; Gallmann, L.; Matuschek, N.; Keller, U. *Science* **1999**, *286*, 1507.
(2) Shirakawa, A.; Sakane, I.; Takasaka, M.; Kobayashi, T. *Appl. Phys. Lett.* **1999**, *74*, 2268.
(3) Song, D. H.; Kambhampati, P.; Kee, T. W.; Barbara, P. F. *J. Phys. Chem. A* **2002**, *106*, 4591.
(4) Rubtsov, I.; Yoshihara, K. In *Femtochemistry*; DeSchryver, F. C., De Feyter, S., Schweiteret, G., Eds.; Wiley: Berlin, 2001.
(5) Engleitner, S.; Seel, M.; Zinth, W. *J. Phys. Chem.* **1999**, *103*, 3013.
(6) Moeller, K. B.; Henriksen, N. L.; Zewail, A. H. *J. Chem. Phys.* **2000**, *113*, 10477.
(7) Wynne, K.; Hochstrasser, R. M. *Adv. Chem. Phys.* **1999**, *106*, 263.
(8) Mahr, H.; Hirsch, M. *Opt. Commun.* **1975**, *13*, 96.
(9) Mokhtari, A.; Chebira, A.; Chesnoy, J. *J. Opt. Soc. Am. B* **1990**, *7*, 1551.
(10) Du, M.; Rosental, S. J.; Xie, X. L.; Diamagno, T. J.; Schmidt, M.; Hanson, D. K.; Schiffer, M.; Norris, J. R.; Fleming, G. R. *Proc. Natl. Acad. Sci. U.S.A.* **1992**, *89*, 8517.
(11) Johnson, A. E.; Jarzeba, W.; Walker, G. C.; Barbara, P. F. *Isr. J. Chem.* **1993**, *33*, 199.
(12) de Boeij, W. P.; Pschenichnikov, M. S.; Wiersma, D. A. *Chem. Phys. Lett.* **1995**, *238*, 1.
(13) Jimenez, R.; Fleming, G. R.; Kumar, P. V.; Maroncelli, M. *Nature* **1994**, *369*, 471.
(14) Dunn, T. J.; Sweetser, J. N.; Walmsley, I. A.; Radzewicz, C. *Phys. Rev. Lett.* **1993**, *70*, 3388.
(15) Wang, H.; Damen, J. S. T. C.; Pfeiffer, L. *Phys. Rev. Lett.* **1995**, *74*, 3065.
(16) Stanley, R. J.; Boxer, S. G. *J. Phys. Chem.* **1995**, *99*, 859.
(17) Akimoto, S.; Yamazaki, I.; Sakawa, T.; Mimuro, M. *J. Phys. Chem. A* **2002**, *106*, 2237.
(18) Kano, H.; Kobayashi, T. *J. Chem. Phys.* **2002**, *116*, 184.
(19) Domcke, W.; Stock, G. *Adv. Chem. Phys.* **1997**, *100*, 1.
(20) Jean, J.; Friesner, R.; Fleming, G. *J. Chem. Phys.* **1992**, 5827.
(21) Jean, J. M. *J. Chem. Phys.* **1996**, *104*, 5638.
(22) Jean, J. *J. Phys. Chem. A* **1998**, *102*, 7549.
(23) Bixon, M.; Jortner, J. *J. Chem. Phys.* **1997**, *107*, 1470.
(24) Wolfseder, B.; Seidner, L.; Domcke, W.; Stock, G.; Seel, M.; Engleitner, S.; Zinth, W. *Chem. Phys.* **1998**, *233*, 323.
(25) Kühn, O.; May, V.; Schreiber, M. *J. Chem. Phys.* **1994**, *101*, 10404.
(26) Egorova, D.; Kühl, A.; Domcke, W. *Chem. Phys.* **2001**, *268*, 105.
(27) Tang, J.; Lin, S. H. *Chem. Phys. Lett.* **1996**, *254*, 6.
(28) Cheche, T. O.; Lin, S. H. *Phys. Rev. E* **2001**, *64*, 061103.
(29) Lucke, A.; Mak, C. H.; Egger, R.; Ankerhold, J.; Stockburger, J.; Grabert, H. *J. Chem. Phys.* **1997**, *107*, 8397.
(30) Casado-Pascual, J.; Denk, C.; Morillo, M.; Cukier, R. I. *J. Chem. Phys.* **2000**, *113*, 11176.
(31) Allen, L.; Eberly, J. *Optical Resonance and Two-Level Atoms*; Dover: New York, 1987.
(32) Reid, P. J.; Silva, C.; Barbara, P. F.; Karki, L.; Hupp, J. T. *J. Phys. Chem.* **1995**, *99*, 2609.
(33) Vos, M. H.; Jones, M. R.; Martin, J.-L. *Chem. Phys.* **1998**, *233*, 179.
(34) Vos, M. H.; Lambry, J. C.; Robles, S. J.; Youvan, D. C.; Breton, J.; Martin, J. L. *Proc. Natl. Acad. Sci. U.S.A.* **1991**, *88*, 8885.
(35) Zimmermann, C.; Willig, F.; Ramakrishna, S.; Burfeindt, B.; Pettinger, B.; Eichberger, R.; Storck, W. *J. Phys. Chem. B* **2001**, *105*, 9245.
(36) Jean, J. M. *J. Chem. Phys.* **1994**, *101*, 10464.
(37) Ungar, L. W.; Cina, J. A. *J. Phys. Chem. A* **1998**, *102*, 7382.
(38) Matro, A.; Cina, J. A. *J. Phys. Chem.* **1995**, *99*, 2568.
(39) Lin, S. H.; Hayashi, M.; Suzuki, S.; Gu, X.; Xiao, W.; Sugawara, M. *Chem. Phys.* **1995**, *197*, 435.
(40) Sugawara, M.; Hayashi, M.; Suzuki, S.; Lin, S. H. *Mol. Phys.* **1996**, *87*, 637.
(41) Hayashi, M.; Yang, T. S.; Mebel, A.; Chang, C. H.; Lin, S. H.; Scherer, N. F. *Chem. Phys.* **1997**, *217*, 259.
(42) Hayashi, M.; Yang, T. S.; Yu, J.; Mebel, A.; Lin, S. H. *J. Phys. Chem. A* **1998**, *102*, 4256.
(43) Chernyak, V.; Minami, T.; Mukamel, S. *J. Chem. Phys.* **2000**, *112*, 7953. Kirkwood, J.; Scheurer, C.; Chernyak, V.; Mukamel, S. *J. Chem. Phys.* **2001**, *114*, 2419.
(44) Okada, A.; Chernyak, V.; Mukamel, S. *J. Phys. Chem. A* **1998**, *102*, 1241.
(45) Mukamel, S. *Principles of Nonlinear Optical Spectroscopy*; Oxford University: New York, 1995.
(46) Ungar, L. W.; Cina, J. A. *Adv. Chem. Phys.* **1997**, *100*, 171.
(47) Eberly, J. H.; Wodkiewicz, K. *J. Opt. Soc. Am.* **1977**, *67*, 1253.
(48) Kowalczyk, P.; Radzewicz, C.; Mostowski, J.; Walmsley, I. A. *Phys. Rev. A* **1990**, *42*, 5622.
(49) Gelin, M. F.; Pisliakov, A. V.; Domcke, W. *Phys. Rev. A* **2002**, *65*, 062507.
(50) Santoro, F.; Petrongolo, C.; Lami, A. *J. Chem. Phys.* **2000**, *113*, 4073.
(51) Marcus, R. A. *J. Chem. Phys.* **1956**, *24*, 966.
(52) Takagahara, T.; Hanamura, E.; Kubo, R. *J. Phys. Soc. Jpn.* **1978**, *44*, 728.
(53) Weiss, U. *Quantum Dissipative Systems*; World Scientific: Singapore, 1993.
(54) Leggett, A. J.; Chakravarty, S.; Dorsey, A. T.; Fisher, M. P. A.; Garg, A.; Zwerger, W. *Rev. Mod. Phys.* **1987**, *59*, 1.
(55) Pollard, W. T.; Felts, A. K.; Friesner, R. A. *Adv. Chem. Phys.* **1996**, *93*, 77.
(56) Redfield, A. G. *Adv. Magn. Reson.* **1965**, *1*, 1.
(57) Blum, K. *Density Matrix Theory and Applications*; Plenum: New York, 1981.
(58) Press, W. H.; Flannery, B. P.; Teukolsky, S. A.; Vetterling, W. T. *Numerical Recipes*; Cambridge University: Cambridge, 1986.
(59) Koeppel, H.; Meyer, H.-D. *Chem. Phys. Lett.* **1984**, *107*, 149.
(60) Stock, G.; Domcke, W. *Chem. Phys.* **1988**, *124*, 227.
(61) Stock, G.; Schneider, R.; Domcke, W. *J. Chem. Phys.* **1989**, *90*, 7184.
(62) Fainberg, B. D. *Opt. Spectrosc.* **1988**, *65*, 722.
(63) Evans, D. G.; Coalson, R. D. *J. Chem. Phys.* **1996**, *104*, 3598.
(64) Ben-Nun, M.; Levine, R. D.; Fleming, G. R. *J. Chem. Phys.* **1996**, *105*, 3035.
(65) Lucke, A.; Ankerhold, J. *J. Chem. Phys.* **2001**, *115*, 4696.
(66) Zusman, L. D. *Chem. Phys.* **1980**, *49*, 295.
(67) Thoss, M.; Wang, H. B. *Chem. Phys. Lett.* **2002**, *358*, 298.
(68) Egorova, D.; Thoss, M.; Domcke, W.; Wang, H. To be published.